Resonance strength in ^{22}Ne(p,γ)^{23}Na from depth profiling in aluminum

R. Longland, C. Iliadis, J. M. Cesaratto, A. E. Champagne, S. Daigle, and J. R. Newton

Department of Physics and Astronomy, University of North Carolina at Chapel Hill, Chapel Hill, North Carolina 27599, USA
and Triangle Universities Nuclear Laboratory, Durham, North Carolina 27708, USA

R. Fitzgerald

National Institute of Standards and Technology, 100 Bureau Drive, Stop 8462, Gaithersburg, Maryland 20899-8462, USA
(Received 10 March 2010; published 21 May 2010)

A novel method for extracting absolute resonance strengths has been investigated. By implanting ^{22}Ne ions into a thick aluminum backing and simultaneously measuring the ^{22}Ne + p and ^{27}Al + p reactions, the strength of the $E_r^{\text{lab}} = 479$ keV resonance in ^{22}Ne(p,γ)^{23}Na was determined to be $\omega\gamma = 0.524(51)$ eV. This result has significantly reduced uncertainties compared to earlier work. Our results are important for the absolute normalizations of resonance strengths in the ^{22}Ne(p,γ)^{23}Na hydrogen-burning reaction and in the ^{22}Ne + α s-process neutron-source reactions.

I. INTRODUCTION

Nuclear reaction rates of many important stellar burning processes are dominated by resonances in the reaction cross section. To improve the accuracy in these rates, in recent evaluations [1,2] resonance strengths have been determined relative to a backbone of accurately measured "standard strengths" [3]. Those strengths have been determined relative to elastic scattering where many systematic effects cancel out, such as those from detector efficiency, beam charge, and target stoichiometry. Standard resonance strengths measured in this way, consequently, depend only on measured count rates and Rutherford scattering cross sections [4–6]. However, as is apparent from Table 1 in Ref. [1], there are no proposed standard resonance strengths for proton-induced reactions involving noble gas targets. The ^{22}Ne + p reaction is one example, which is important for hydrogen burning, particularly in the Ne-Na cycle.

Many resonance strengths for capture reactions involving noble gases have been measured previously using implanted targets, where in most cases the target backing material was a thin ($\approx$0.5 mm thick) tantalum sheet. In reactions such as ^{22}Ne + p, it is notoriously difficult to obtain absolute strengths since the stoichiometry of the implanted region must be known to extract a strength from a thick-target excitation function. There is currently one measured absolute strength in ^{22}Ne(p,γ)^{23}Na corresponding to the $E_r^{\text{lab}} = 1278$ keV resonance [7]. For this resonance, the stoichiometry of the implanted ^{22}Ne targets was obtained with Rutherford backscattering but the measurement has never been independently verified. In addition, this resonance is beyond the reach of most low-energy accelerators, necessitating the need for a standard resonance strength at low energy.

Here, we report on an absolute resonance strength measurement of the $E_r^{\text{lab}} = 479$ keV resonance in ^{22}Ne(p,γ)^{23}Na. The experiment utilizes a target composed of ^{22}Ne ions implanted into an aluminum substrate. By measuring the well-known $E_r^{\text{lab}} = 406$ keV resonance in ^{27}Al(p,γ)^{28}Si and the $E_r^{\text{lab}} = 479$ keV resonance in ^{22}Ne(p,γ)^{23}Na simultaneously, the absolute strength of the latter resonance can be obtained independently from the knowledge of absolute beam currents, absolute detector efficiencies, or the stoichiometry of the target. Obtaining a resonance strength independently of the target stoichiometry is a significant advantage of this method. Our new method is not specific to ^{22}Ne(p,γ)^{23}Na, but it could also be useful for other reactions. Note that an accurately measured ^{22}Ne(p,γ)^{23}Na resonance strength will also improve estimates of the ^{22}Ne + α rates, since the targets for the latter case were previously characterized using ^{22}Ne + p resonances [8].

A theoretical outline of our new method is given in Sec. II. The experimental equipment used to perform the depth profiling of ^{22}Ne in aluminum is described in Sec. III. The procedure for measuring the target profile and a discussion of specific analysis techniques used are given in Sec. IV. The results are presented and discussed in Sec. V, and conclusions are given in Sec. VI. Throughout this work, kinematic quantities are given in the center-of-mass reference frame, unless stated otherwise.

II. EXCITATION FUNCTIONS FROM NUCLEAR RESONANCES

An excitation function for a nuclear reaction is obtained by measuring the yield over a range of incident beam energies. The measured yield is defined as

$$\text{yield} = \frac{\text{number of reactions}}{\text{number of incident particles}}. \quad (1)$$

For a capture reaction, the experimental yield (Y) can be calculated by measuring the intensity of γ rays with a germanium detector:

$$Y = \frac{e}{\varepsilon^p W(\theta) B} \frac{I}{Q}, \quad (2)$$

where e is the fundamental electric charge, ε^p is the full-energy peak efficiency for the measured γ ray, $W(\theta)$ is the angular

correlation function at detector angle θ with respect to the beam direction, B is the cross-section fraction that is carried by the observed γ ray (e.g., the branching ratio for a primary transition), I is the number of counts observed in the full-energy peak, and Q is the measured beam charge accumulated on the target.

The yield depends on the measured cross section as well as on the nature of the target containing the reacting nuclei. Understanding the effect of the target on the measured yield is critical for extracting resonance strengths or cross sections from excitation functions. For a target with a varying ion concentration with depth, the yield will depend on the location in the target where the reactions occur. For narrow resonances, most of the reactions will occur at a depth determined by the incident beam energy and the energy loss in the target. A finite beam resolution and energy straggling in the target serve to broaden the excitation function.

The excitation function resulting from a varying ion concentration at different target depths can be described by dividing the target into many thin depth slices. By using this approximation, the yield from a nuclear reaction is obtained from a sum over the contributions of each layer, i, of the target [9]:

$$Y(E_0) \approx \sum_i N_i F_i(E_0). \tag{3}$$

Here, E_0 is the mean beam energy, N_i is the target atom concentration in each layer (in units of nuclei per square centimeter), and $F_i(E_0)$ is the convolution function of the cross section, $\sigma(E)$, beam energy profile, and energy straggling in the target [9]:

$$F_i(E_0) = \int_{E'=0}^{E_0} g_i(E_0 - E') dE' \int_{E=-\infty}^{\infty} \sigma(E) h(E' - E) dE. \tag{4}$$

The beam spread function, $h(E' - E)dE$, is expected to be Gaussian in shape, and it describes the probability of a beam particle having an energy between E and $E + dE$ at a depth corresponding to an energy of $E' = E_0 - \Delta E$. The cross section at negative energies is zero, permitting the integral over negative energies, E. The straggling function, $g_i(E_0 - E')dE'$ (defined at each layer i), describes the probability of a beam particle losing energy to result in an energy between E' and $E' + dE'$ at a depth of x_i. Straggling effects can be computationally intensive to calculate [9,10]. However, beam particles typically undergo many collisions with electrons, losing several keV of energy in the thick stopping targets used in nuclear astrophysics experiments. In these cases, the central limit theorem of statistics states that energy straggling can also be approximated by a Gaussian function [10]. Thus we assume

$$h(E' - E) = \frac{1}{\sqrt{2\pi}\sigma_b} \exp\left[-\frac{(E' - E)^2}{2\sigma_b^2}\right], \tag{5}$$

$$g_i(E_0 - E') = \frac{1}{\sqrt{2\pi x_i}\sigma_s} \exp\left[-\frac{(E_0 - E' - \Delta_i)^2}{2\sigma_s^2 x_i}\right]. \tag{6}$$

The adjustable parameters σ_b and σ_s define the beam energy width and straggling rate, respectively. The average energy

loss of the beam particles at depth x_i is denoted by Δ_i and is given by the integral (sum) of the total linear stopping power, dE/dx, up to that location:

$$\Delta_i = \sum_{j=1}^{i} (x_j - x_{j-1}) \frac{dE}{dx_j}. \tag{7}$$

In previous work a constant total linear stopping power was frequently assumed [9]. This is only valid if (i) the beam does not lose too much energy in the target so that the stopping power for pure layers is nearly energy independent and (ii) the ion concentrations do not vary significantly over the depth of the target. For example, if a given species is implanted in high doses, resulting in a strongly varying depth concentration, then the second assumption is not valid, and the total stopping power of the material cannot be assumed to be constant, even if the energy lost in the target is relatively small.

For a sample produced by implanting species p into a substrate of species q, the energy lost per unit path length is given by

$$\frac{dE}{dx} = N_q S_q + N_p S_p = N_A \left[\frac{\rho_q}{M_q} S_q + \frac{\rho_p}{M_p} S_p\right], \tag{8}$$

where N is the number of atoms per cubic centimeter, S is the stopping cross section (eV cm^2/atom), N_A is Avogadro's number, M is the atomic mass in amu, and the mass density (in g/cm^3) of atoms is given by ρ. In general, the stopping cross sections depend on energy. To determine the densities ρ, the nature of the implanted region must be known. Here, we assume that the implanted atoms are located in interlattice spacings, resulting in an overall material density increase:

$$\rho_q(x_i) = \overline{\rho_q} = \text{constant}, \tag{9}$$

$$\rho_p(x_i) = \xi(x_i) \frac{\overline{\rho_q} M_p}{M_q}, \tag{10}$$

where $\xi(x_i)$ is the stoichiometry (i.e., the number ratio of implanted to substrate atoms, N_p/N_q) at depth x_i and $\overline{\rho_q}$ is the mean density of the pure substrate material (without species p).

Depth profiling is usually performed with narrow nuclear resonances, whose peaked shapes provide sufficient depth resolution. In the present work, the measured resonances have total widths on the order of tens of electron volts [11,12]. Narrow-resonance cross sections, for which the partial widths can be assumed to be energy independent over the total resonance width, can be described by the Breit-Wigner formula

$$\sigma(E) = \frac{\lambda^2}{4\pi} \omega \frac{\Gamma_a \Gamma_b}{(E - E_r)^2 + \Gamma^2/4} \tag{11}$$

$$= \frac{\lambda^2}{4\pi} \omega \gamma \Gamma \frac{1}{(E - E_r)^2 + \Gamma^2/4}, \tag{12}$$

with

$$\omega = \frac{(2j + 1)}{(2j_p + 1)(2j_t + 1)}, \tag{13}$$

where Γ_a, Γ_b, and Γ are the entrance particle partial width, exit photon partial width, and the total width, respectively; E_r is the resonance energy; j, j_p, and j_t are the spin of the

resonance, projectile, and target nucleus, respectively; and $\omega\gamma$, the resonance strength, is

$$\omega\gamma = \omega\frac{\Gamma_a\Gamma_b}{\Gamma}. \tag{14}$$

If the resonance used for depth profiling is sufficiently narrow with respect to the beam energy spread (i.e., $\Gamma \ll \sigma_b$), the convolution of cross section and beam spread functions in Eq. (4) can be simplified to

$$\int_{E=-\infty}^{\infty} dE\sigma(E)h(E'-E)$$
$$= \frac{\lambda^2}{4\pi}\omega\gamma\Gamma\int_{E=-\infty}^{\infty} dE\frac{h(E'-E)}{(E-E_r)^2+\Gamma^2/4}$$
$$= \frac{\lambda^2}{2}\omega\gamma h(E'-E_r). \tag{15}$$

For the assumption of a narrow resonance, the yield in Eqs. (3) and (4) can then be written as

$$Y(E_0) = \frac{\lambda^2}{2}\omega\gamma\sum_i N_i\frac{1}{2\pi\sigma_b\sigma_s\sqrt{x_i}}\int_{E'=0}^{E_0} dE'$$
$$\times \exp\left[-\frac{(E'-E_r)^2}{2\sigma_b^2}\right]\exp\left[-\frac{(E_0-E'-\Delta_i)^2}{2\sigma_s^2 x_i}\right]. \tag{16}$$

In the present work, we implanted ^{22}Ne ions into a thick aluminum sheet and measured the yields of the narrow resonances at $E_r^{\rm lab} = 406$ keV in ^{27}Al$(p,\gamma)^{28}$Si and at $E_r^{\rm lab} = 479$ keV resonance in ^{22}Ne$(p,\gamma)^{23}$Na simultaneously. For both resonances, the yield is given by Eq. (16). In the following, we will denote the implanted species ($p = {}^{22}$Ne) by the subscript 22 and the substrate species ($q = {}^{27}$Al) by the subscript 27.

Since the implanted ^{22}Ne ions are concentrated near the surface of the aluminum sheet, we expect a well-defined peak shape for the ^{22}Ne + p yield curve. In contrast, the ^{27}Al + p yield curve will reveal an interesting structure. In the pure aluminum region, beyond the implanted ^{22}Ne depth, the ^{27}Al + p yield will be at a maximum [$\rho_{22} = 0$ in Eq. (8)]. However, in the ^{22}Ne implanted region we have $\rho_{22} \neq 0$ and thus the energy loss, Δ_i, in Eq. (16) increases, resulting in a smaller yield. Therefore, we expect a step in the excitation function caused by the implanted region near the surface of the target. The situation is shown schematically in Fig. 1.

The general strategy was the following: (i) Fit Eq. (16) to the measured ^{27}Al + p yield curve, including the step on the front edge; this allowed us to extract the stoichiometry, $\xi(x) = N_{22}/N_{27}$ [which enters through Eqs. (7)–(10)] together with the absolute normalization of the yield. (ii) With the stoichiometry $\xi(x)$ and the absolute yield normalization factor determined from the previous step, Eq. (16) was fit to the measured ^{22}Ne + p yield curve. The resonance strength in ^{22}Ne + p is left as a free parameter to be extracted from the fit.
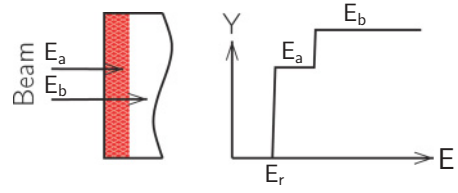

FIG. 1. (Color online) Schematic showing the effect of implanting neon atoms into an aluminum substrate. Incident protons with energies E_a are captured by ^{27}Al nuclei in the implanted region, which is close to the surface of the target. The increased total stopping cross section in this region leads to a decreased yield [Eq. (16)]. Beams with energies of E_b react deeper inside the target in a region of pure aluminum. The yield at these energies is higher compared to the implanted region. Note, however, that for a given incident energy the depth of a reaction occurring in a region of pure aluminum will be affected by the energy loss (or total stopping power) in the implanted region.

III. EXPERIMENTAL EQUIPMENT

A. Implanted target

The backing used for the experiment was a 1-mm-thick aluminum sheet (99% purity). The backing was cleaned thoroughly with acetone and ethanol before implantation. An Eaton ion implanter with a modified end station (located at the University of North Carolina at Chapel Hill) was used to implant ^{22}Ne ions into this backing. The ion implanter accelerated neon ions from a pressurized natural neon ($9.25\% \pm 0.03\%$ molar fraction of ^{22}Ne) gas bottle to an energy of 100 keV. A $90°$ analyzing magnet (with a quoted selectivity of $1/100$) was used to mass separate the ^{22}Ne ions. The incident dose of ^{22}Ne was estimated by integrating the beam current on the backing, assuming singly charged incident ^{22}Ne ions. The beam current on the backing amounted to about 20 μA on average. The total accumulated charge was 0.26 C (corresponding to 1.6×10^{18} incident ^{22}Ne ions) over a circular implantation region of 2.5 cm in diameter. A liquid-nitrogen-cooled trap reduced contamination buildup (such as carbon and fluorine) on the backing.

B. Setup

Depth profiling of the implanted aluminum backing was conducted at the Laboratory for Experimental Nuclear Astrophysics (LENA), located at the Triangle Universities Nuclear Laboratory. A 1-MV Van de Graaff accelerator was used to accelerate proton beams to energies in the range of $E_p = 400$–505 keV with a total integrated beam charge on target of ≈ 0.13 C over a beam spot of about 1 cm in diameter. Secondary-electron suppression was applied for the beam current measurement. In addition, a liquid-nitrogen-cooled trap reduced contaminant buildup on the target surface. The beam current was kept to a minimum (≈ 5 μA) to ensure that the target did not degrade.

C. Detector

Capture γ rays from the excited compound nuclei (^{28}Si and ^{23}Na) were detected using a 135% relative efficiency HPGe
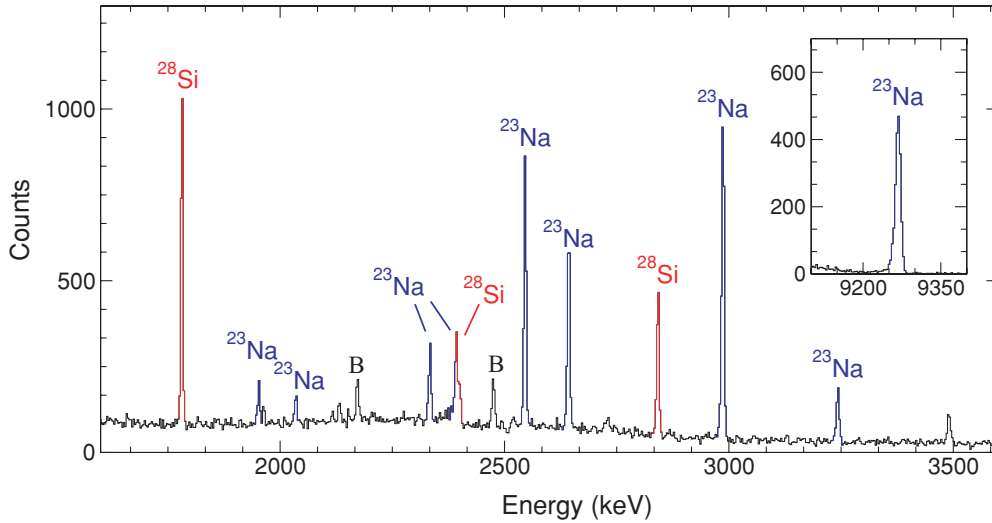
FIG. 2. (Color online) Sample γ-ray spectrum, obtained at a beam energy of 490 keV with an accumulated charge of 2×10^{-3} C on target. The target consisted of ^{22}Ne ions implanted into aluminum and thus resonances in the ^{27}Al$(p,\gamma)^{28}$Si and ^{22}Ne$(p,\gamma)^{23}$Na reactions were excited simultaneously. Major peaks are labeled by the decaying nucleus (^{23}Na in blue; ^{28}Si in red); the label "B" denotes background. The inset shows the peak corresponding to the ground-state transition $(9253 \to 0)$ for the ^{22}Ne$(p,\gamma)^{23}$Na reaction.

detector. The detector was located at $55°$ with respect to the beam direction at a distance of 3.0 cm from the center of the target. The target and detector were surrounded by at least 5 cm of lead in all directions to reduce background caused by environmental sources and from x rays produced by the accelerator.

The energy signals from the detector were amplified with an Ortec 572 spectroscopy amplifier and recorded with a CAEN 785 ADC. Detector dead times were monitored with an Ortec 448 precision pulse generator throughout the experiment and were kept below 3%.

The detector efficiencies, used both for peak intensity normalization and for summing corrections, were obtained by three methods: radioactive source measurements, resonant (p,γ) reactions, and Monte Carlo simulations using GEANT4 [13]. First, the sum-peak method [14] was used with ^{60}Co to find the absolute full-energy peak and total efficiencies at $E_\gamma = 1173$ and 1332 keV that do not depend on knowledge of the absolute source activity. Subsequently, other radioactive sources (^{56}Co and ^{152}Eu) were used to obtain relative full-energy peak efficiencies up to $E_\gamma = 3.5$ MeV. The $E_r^{\text{lab}} = 278$ keV resonance in ^{14}N$(p,\gamma)^{15}$O was used to extend the full-energy peak efficiency curve to $E_\gamma = 7.5$ MeV. It is important to note that because of the close detector geometry, all experimental full-energy peak efficiencies must be corrected for coincidence summing effects. The corrections were performed using the code LENASUM [15], which is based on the formulation described in Ref. [16]. Following the experimental determination of full-energy peak efficiencies, the experimental data points were interpolated using GEANT4 simulations. These simulations have been shown to be accurate to 1.6% between 4.4 and 11.7 MeV for relative efficiencies [17]. Total detection efficiencies, which were needed for coincidence summing corrections, were also obtained with GEANT4 and normalized to the ^{60}Co data.

IV. PROCEDURE AND ANALYSIS

A. Yield curves

Yield curves were measured simultaneously for the ^{27}Al$(p,\gamma)^{28}$Si $(Q = 11585.1$ keV) and ^{22}Ne$(p,\gamma)^{23}$Na $(Q = 8794.1$ keV) reactions at incident proton energies of $E_p^{\text{lab}} = 400$–505 keV. A sample γ-ray spectrum, obtained at an incident beam energy of $E_r^{\text{lab}} = 490$ keV, is shown in Fig. 2. The observed in-beam γ rays arise from the narrow resonances at $E_r^{\text{lab}} = 406$ keV in ^{27}Al$+ p$ and at $E_r^{\text{lab}} = 479$ keV in ^{22}Ne$+ p$.

The ^{27}Al$+ p$ resonance has a target spin of $j = 5/2$ and thus the angular correlation is expected to be approximately isotropic. Considering, in addition, that the detector was located at $\theta_\gamma = 55°$, where the Legendre polynomial $P_2(\cos\theta) = 0$, we can safely adopt an angular correlation factor of $W_{27}(\theta) = 1$ in Eq. (2). Additionally, the ^{22}Ne$+ p$ resonance at $E_r^{\text{lab}} = 479$ keV has a spin of $j = 1/2$ and thus $W_{22}(\theta)$ in Eq. (2) is unity.

1. $^{27}Al(p,\gamma)^{28}Si$

The $E_r^{\text{lab}} = 405.5(3)$ keV resonance $[\omega\gamma = 8.63(52) \times 10^{-3}$ eV] [4] was used to measure the ^{27}Al$(p,\gamma)^{28}$Si yield curve.[1] Relatively small beam currents (≈ 5 μA) were required to avoid damage to the target. The resulting low counting statistics for the primary transitions were insufficient for reliable depth profiling, so the much stronger secondary decay from the first excited state (1779 keV$\to$ 0), which carries 98% of the decay strength, was used for this purpose. The disadvantage

---

[1]The ^{27}Al $+ p$ resonance strengths used in the present work are adopted from Ref. [18]. In that work, the measured strengths (including those from Refs. [20] and [21]) were normalized to the absolute strength standard in Ref. [4].

of monitoring secondary decays in a measurement with an infinitely thick target (i.e., all beam particles stop in the aluminum) is that lower energy resonances in ^{27}Al + p may contaminate the measured yield. The $E_r^{\text{lab}} = 326$ keV resonance in ^{27}Al + p resonance ($\omega\gamma = 1.8(1) \times 10^{-3}$ eV [18]) is of particular importance and had to be accounted for. This was achieved by calculating the expected maximum yield for an infinitely thick target using Eq. (2). The expected contribution to the total 1779 keV$\rightarrow 0$ intensity was then estimated using the branching ratios from Ref. [19] and amounted to about 16% of the maximum yield. This contribution to the decay strength was subtracted from the measured intensities. Note that the first data point in the ^{27}Al + p yield curve is consistent with zero, validating this method of subtracting contamination from other resonances. Another resonance in ^{27}Al + p at $E_r^{\text{lab}} = 447$ keV ($\omega\gamma = 1.50(13) \times 10^{-3}$ eV [18]) had to be considered as well. The angular correlation factor in these corrections is expected to be unity for the same reasons as described previously. To avoid fitting the cumulative yield from two ^{27}Al + p resonances ($E_r^{\text{lab}} = 406$ keV and $E_r^{\text{lab}} = 447$ keV) simultaneously, data points near the higher energy resonance from $E_p^{\text{lab}} = 445$ to 475 keV were removed from the analysis. The expected yield of the $E_r^{\text{lab}} = 447$ keV resonance was then subtracted from data points above $E^{\text{lab}} = 475$ keV. The resulting yield curve, after these corrections have been applied, is shown in Fig. 3(a) and will be discussed later.

2. ^{22}Ne(p,γ)^{23}Na

The primary ground-state transition of the $E_r^{\text{lab}} = 479.3(8)$ keV resonance in ^{22}Ne(p,γ)^{23}Na [11] was used to measure the yield curve shown in Fig. 3(b). The yield was calculated with Eq. (2) and an absolute normalization determined from the ^{27}Al + p yield curve. For the branching ratio of the ground-state transition (9253 keV$\rightarrow 0$) we adopted the results of the literature [22,23], which are in mutual agreement [$B_{22} = 0.465(23)$].

3. Yield curve analysis

The predicted step close to the front edge of the ^{27}Al + p yield curve [Fig. 3(a)], resulting from the ^{22}Ne concentration near the target surface, is clearly observed. The ^{22}Ne + p yield curve [Fig. 3(b)], in contrast, shows a smooth peak, consistent with expectations (Sec. II). Deviation from the expected step shape (Fig. 1) in Fig. 3(a) and the sharp front edge at $E^{\text{lab}} = 479$ keV in Fig. 3(b) are because the ^{22}Ne was not implanted in a uniform layer at the front of the target, but rather in a varying concentration with depth as shown in Fig. 4. It should be noted that an approximately 40-nm-thick layer of aluminum oxide [24] will affect the shape of the yield curves. A SRIM calculation reveals that the energy loss difference between the oxide and pure aluminum is less that 0.5 keV, and therefore outside the resolution of our experiment. The effect of the oxide layer is lessened because of the low ^{22}Ne density close to the surface of the aluminum substrate (see Fig. 4).

A code was written to fit Eq. (16) to the measured yield curves. The least-squares fitting method of McGlone and Johnson [25] was used to determine the depth profile of ^{22}Ne implanted into Al. The concentration profile of implanted
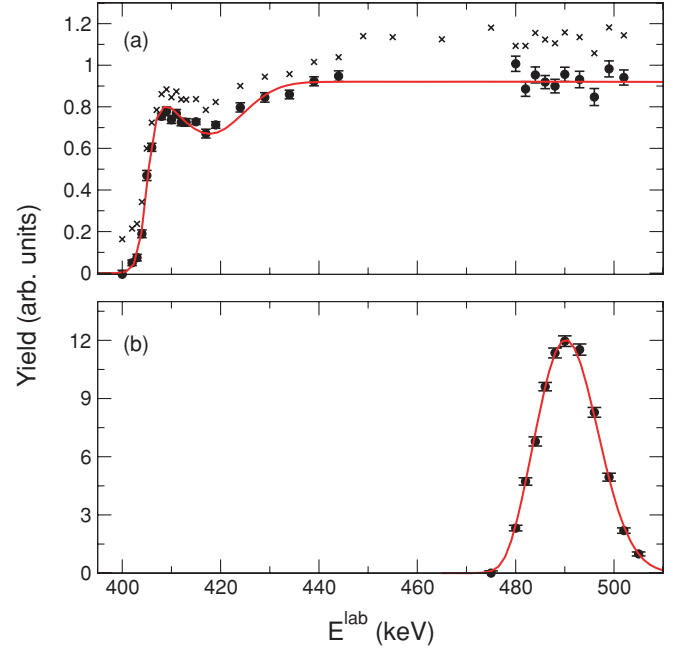

FIG. 3. (Color online) Best fits to the ^{27}Al + p and ^{22}Ne + p yields. (a) Best fit to the $E_r^{\text{lab}} = 406$ keV resonance in ^{27}Al(p,γ)^{28}Si. The absolute yield height data (solid circles) have been corrected for other contaminant resonances as discussed in Sec. IV A1 (uncorrected points are identified with the symbol x). The yield normalization A in Eq. (18) is extracted from the measured yield points above $E^{\text{lab}} = 480$ keV. (b) Best fit to the $E_r^{\text{lab}} = 479$ keV resonance in ^{22}Ne(p,γ)^{23}Na. The absolute height of the yield curve is left as a free parameter in the fit, which determines the resonance strength. Note that there are more high-energy data points in the ^{22}Ne + p yield curve than in the ^{27}Al + p yield curve. This is because the ^{27}Al + p points were removed by contamination from other resonances (see Sec. IV A1). These contaminants do not affect the ^{22}Ne + p yield.

atoms was constrained to a smoothly varying function by adding corrections to the log-likelihood function. The log-likelihood function for a profile grid of M slices, which are fit to N data points, is given by

$$\chi^2 = \chi^2_{\text{data}} + \sum_{j=N+1}^{N+M+1-B} \left[W_{j-N} \sum_{b=1}^{B} N_{22_{j-N+b-1}} P_b \right], \quad (17)$$

where

$$\chi^2_{\text{data}} = \sum_i \frac{(x_i - \overline{x})^2}{\sigma_i^2}.$$

Here, χ^2_{data} is the log-likelihood function calculated from the deviation of fitted points, $\overline{x}$, to experimental points, x_i, assuming uncertainties of σ_i in the data; N_{22_k} denotes the ^{22}Ne ion concentration at each grid point; B and P_k are fixed parameters for controlling the smoothness of the profile; and W_k are weights, which were adjusted manually to control the smoothness of the profile. As in Ref. [25], we
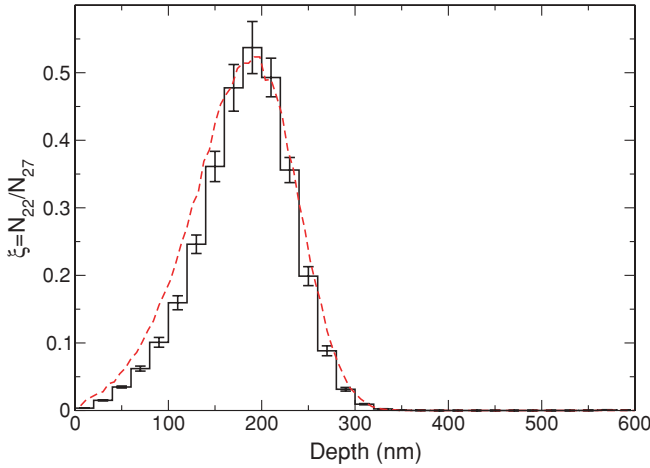
FIG. 4. (Color online) Stoichiometry profile, $\xi(x)$, of implanted ^{22}Ne ions in the aluminum backing as obtained from a fit to the ^{27}Al + p yield curve in Fig. 3(a). The concentration profile simulated with SRIM, which is normalized to the maximum height of the data points, is shown as a dashed line.

choose $B = 4$ and $P_b = -1, 3, -3, 1$ to obtain a quadratic smoothness between every four points with $W = 20$.[2]

The strength of the $E_r^{\mathrm{lab}} = 479$ keV resonance in ^{22}Ne$(p,\gamma)^{23}$Na was determined from the following procedure (outlined already in Sec. II). We started with the yield for the ^{27}Al + p reaction, which is given by Eqs. (2) and (16) as

$$
Y_{27}(E_0) = A \left(\frac{1}{\varepsilon_{27}^p Q_{27}} \right)_{\mathrm{rel}} \frac{e}{B_{27}} I_{27}(E_0)
$$

$$
= \omega\gamma_{27} \frac{\lambda_r^2}{2\pi\sigma_b\sigma_s} \sum_i N_{27_i} \frac{1}{\sqrt{x_i}} \int_{E'=0}^{E_0} dE'
$$

$$
\times \exp\left[-\frac{(E' - E_r)^2}{2\sigma_b^2} \right] \exp\left[-\frac{(E_0 - E' - \Delta_i)^2}{2\sigma_s^2 x_i} \right],
$$
(18)

where $(\varepsilon_{27}^p Q_{27})_{\mathrm{rel}}$ is the product of the relative peak efficiency and relative accumulated charge, and A denotes their combined absolute normalization factor. The absolute strength of the $E_r^{\mathrm{lab}} = 406$ keV resonance is labeled by $\omega\gamma_{27}$. From the measured ^{27}Al + p yield curve [Fig. 3(a)], the fitting parameters A, and $\xi(x)$ (affecting the energy loss Δ_i) were extracted.

The stoichiometry, $\xi = N_{22}/N_{27}$, as a function of depth that was extracted by fitting the ^{27}Al + p yield is shown in Fig. 4. The stoichiometry profile is overlaid with the simulated profile (dashed line) of 100-keV ^{22}Ne ions implanted into an aluminum substrate, as obtained from the Monte Carlo ion transport code SRIM [28]. There is reasonable agreement between measured and simulated ^{22}Ne depth profiles. Note

that the maximum stoichiometry amounts to a Ne:Al ratio of 1:2.

Once the stoichiometry profile, ξ, and constant, A, were extracted from the ^{27}Al + p yield curve, the ^{22}Ne + p yield curve was fit. The ^{22}Ne + p yield is given by

$$
Y_{22}(E_0) = A \left(\frac{1}{\varepsilon_{22}^p Q_{22}} \right)_{\mathrm{rel}} \frac{e}{B_{22}} I_{22}(E_0)
$$

$$
= \omega\gamma_{22} \frac{\lambda_r^2}{2\pi\sigma_b\sigma_s} \sum_i N_{22_i} \frac{1}{\sqrt{x_i}} \int_{E'=0}^{E_0} dE'
$$

$$
\times \exp\left[-\frac{(E' - E_r)^2}{2\sigma_b^2} \right] \exp\left[-\frac{(E_0 - E' - \Delta_i)^2}{2\sigma_s^2 x_i} \right].
$$
(19)

At this stage, the only fitting parameter is the strength of the ^{22}Ne + p resonance, $\omega\gamma_{22}$. There are several advantages of using the method outlined here. First, only relative detector efficiencies need to be known in Eq. (19). These relative efficiencies have been shown in Ref. [17] to be accurate to within a few percent. Second, only the relative accumulated charge needs to be known. Note that above $E^{\mathrm{lab}} = 480$ keV the same runs were used to analyze the ^{22}Ne + p and ^{27}Al + p yields, and thus the beam charge, Q, cancels completely. Fitting Eq. (19) to the measured yield shown in Fig. 3(b) gave the strength of the $E_r^{\mathrm{lab}} = 479$ keV resonance in ^{22}Ne + p, for which we find a value of $\omega\gamma = 0.524(51)$ eV.

The uncertainty budget for the extracted strength of the $E_r^{\mathrm{lab}} = 479$ keV resonance in ^{22}Ne + p is presented in Table I. The uncertainty in the reference resonance strength ($E_r^{\mathrm{lab}} = 406$ keV in ^{27}Al + p) is 6% [4]. The GEANT4 simulations used for relative detector efficiencies are shown to be accurate to within a few percent for extrapolation in the energy range $E_\gamma = 4$–11 MeV [17]. Relative uncertainties of 2% were therefore assigned to detection efficiencies. Literature values for the primary branching ratios in ^{22}Ne + p contribute 5% to the resonance strength uncertainty. Stopping power uncertainties in the energy regions of interest were estimated from the data compiled on the SRIM Web site [28]. The stopping power uncertainty for ^{27}Al + p and ^{22}Ne + p were estimated to be 4% and 3%, respectively. The stopping powers affect the yield of both ^{27}Al + p and ^{22}Ne + p yield curves through Eq. (7). Since the energy loss enters in the exponential of Eqs. (18) and (19), the importance of the stopping power uncertainties is lessened, resulting in resonance strength uncertainty contributions of just 2% and 1%, respectively.

TABLE I. Uncertainty budget for the extracted $E_r^{\mathrm{lab}} = 479$ keV resonance strength in ^{22}Ne + p.

Source	Uncertainty in $\omega\gamma_{22}$ (%)
Reference ^{27}Al + p strength	6
Relative efficiencies	2
Branching ratios	5
Stopping powers (Al)	2
Stopping powers (Ne)	1
Fitting	5
Total	10

---

[2]A two-step minimization was employed to find the best-fit depth profile. The Broyden-Fletcher-Goldfarb–Shanno (BFGS) method [26] was used for the initial parameter search, and the Nelder-Mead gradient based search [27] was adopted to finely tune the minimization. Finite-difference second derivatives were employed to estimate uncertainties in the fit parameters.
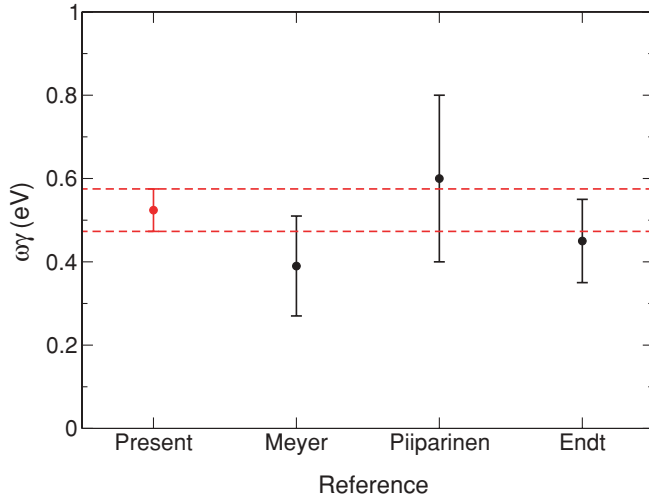
FIG. 5. Comparison of present result (shown in red) for the $E_r^{\text{lab}} = 479$ keV resonance strength in ^{22}Ne$(p,\gamma)^{23}$Na to previously published results. The labels Meyer, Piiparinen, and Endt refer to Refs. [22], [23], and [11], respectively.

In addition to uncertainties affecting the resonance strength, the effect of a different implantation model was investigated. In this model, the implanted ^{22}Ne atoms replaced aluminum atoms during implantation, resulting in a constant number density for the implanted material. Equations (9) and (10) are then replaced by

$$\rho_{27}(x_i) = \overline{\rho_{27}} \left[1 - \xi(x) \right], \tag{20}$$

$$\rho_{22}(x_i) = \xi(x_i) \frac{\overline{\rho_{27}} M_{22}}{M_{27}}. \tag{21}$$

This model was found to only affect the width of the extracted profile, whereas the total number of implanted nuclei and hence the resonance strength $\omega\gamma_{22}$ remain approximately constant. All uncertainties were summed in quadrature. The total uncertainty in the extracted $E_r^{\text{lab}} = 479$ keV resonance strength in ^{22}Ne$(p,\gamma)^{23}$Na amounted to 10%.

V. DISCUSSION

All previously measured strengths for the $E_r^{\text{lab}} = 479$ keV resonance in ^{22}Ne $+ p$ were normalized relative to higher lying resonances in the ^{22}Ne $+ p$ reaction. In our work, we have obtained the resonance strength independently of other resonances in ^{22}Ne $+ p$, with no dependence on absolute detector efficiencies or absolute beam charge integration. A comparison of the new result with values derived from the literature is shown in Fig. 5.

The value obtained by Meyer and Smit [22] was normalized to the ^{22}Ne $+ p$ $E_r^{\text{lab}} = 640$ keV resonance strength from Ref. [29]. The rather large uncertainty is dominated by the uncertainty of that reference resonance. The value of $\omega\gamma =$

0.45(10) eV ($\pm 20\%$) in Endt [11], however, was obtained by normalizing the resonance strengths from Meyer to the absolute strength of the ^{22}Ne $+ p$ $E_r^{\text{lab}} = 1278$ keV resonance reported by Keinonen *et al.* [7]. Another relative measurement was performed by Piiparinen *et al.* [23], but unfortunately, no uncertainties are quoted for the relative yield of the $E_r^{\text{lab}} = 479$ keV resonance. For comparison, we assumed a relative yield uncertainty of 30% (considering their statement that relative yield uncertainties were between 10% and 50%), and we normalized their strength to the result from Keinonen *et al.* [7]. As is apparent from Fig. 5, we have significantly improved the uncertainty of the $E_r^{\text{lab}} = 479$ keV resonance strength in ^{22}Ne $+ p$ from a previous value near 30% to 10%. Our new technique removes any systematic uncertainty from the target stoichiometry, which is difficult to quantify using traditional methods.

It was already mentioned in the introduction that our new value for the $E_r^{\text{lab}} = 479$ keV resonance strength in ^{22}Ne $+ p$ is important in two respects. First, it will reduce the rate uncertainties of the ^{22}Ne$(p,\gamma)^{23}$Na reaction since the strengths of the low-energy resonances can be renormalized relative to our precisely measured strength for $E_r^{\text{lab}} = 479$ keV and thus will improve predictions of hydrogen-burning nucleosynthesis. Second, our precise strength can be used to determine more reliable stoichiometries for implanted ^{22}Ne-Ta targets that have been employed in measurements of the important ^{22}Ne$(\alpha,\gamma)^{26}$Mg and ^{22}Ne$(\alpha,n)^{25}$Mg s-process neutron source reactions. New thermonuclear reaction rates for ^{22}Ne $+ p$ and ^{22}Ne $+ \alpha$ will be published elsewhere.

VI. SUMMARY

A novel method for measuring reliable resonance strengths has been employed. By implanting ^{22}Ne ions into a thick aluminum backing, and simultaneously measuring the ^{22}Ne $+ p$ and ^{27}Al $+ p$ reactions, the strength of the $E_r^{\text{lab}} = 479$ keV resonance in ^{22}Ne$(p,\gamma)^{23}$Na was determined to be $\omega\gamma = 0.524(51)$ eV. Our formalism allows for finding the implantation profile of ^{22}Ne in a thick aluminum target backing. This novel approach significantly reduced uncertainties in the desired resonance strength owing to the cancellation of several systematic experimental uncertainties. The well-known $E_r^{\text{lab}} = 406$ keV resonance in ^{27}Al$(p,\gamma)^{28}$Si was used as a reference. Our new precise value for the ^{22}Ne $+ p$ resonance strength is important for estimating reliable thermonuclear reaction rates for the hydrogen burning of ^{22}Ne and for the normalization of the ^{22}Ne $+ \alpha$ s-process reactions.

[1] C. Iliadis, J. M. D'Auria, S. Starrfield, W. J. Thompson, and M. Wiescher, Astron. Phys. J. Suppl. **134**, 151 (2001).

[2] R. Longland *et al.*, Nucl. Phys. A (2010) doi:10.1016/j.nuclphysa.2010.04.008.

[3] C. Iliadis, *Nuclear Physics of Stars* (Wiley-VCH, New York, 2007).

[4] D. C. Powell, C. Iliadis, A. E. Champagne, S. E. Hale, V. Y. Hansper, R. A. Surman, and K. D. Veal, Nucl. Phys. A **644**, 263 (1998).

[5] C. Rowland, C. Iliadis, A. E. Champagne, and J. Mosher, Phys. Rev. C **65**, 064609 (2002).

[6] B. M. Paine and D. G. Sargood, Nucl. Phys. A **331**, 389 (1979).

[7] J. Keinonen, M. Riihonen, and A. Anttila, Phys. Rev. C **15**, 579 (1977).

[8] U. Giesen *et al.*, Nucl. Phys. A **561**, 95 (1993).

[9] B. Maurel, G. Amsel, and J. Nadai, Nucl. Instrum. Methods **197**, 1 (1982).

[10] R. P. Pezzi, C. Krug, P. L. Grande, E. B. O. da Rosa, G. Schiwietz, and I. J. R. Baumvol, Appl. Phys. Lett. **92**, 164102 (2008).

[11] P. M. Endt, Nucl. Phys. A **521**, 1 (1990).

[12] P. M. Endt, Nucl. Phys. A **633**, 1 (1998).

[13] S. Agostinelli *et al.* (GEANT4 Collaboration), Nucl. Instrum. Methods A **506**, 250 (2003).

[14] I. Kim, C. Park, and H. Choi, Appl. Rad. Isotopes. **58**, 227 (2003).

[15] R. Longland, C. Iliadis, A. E. Champagne, C. Fox, and J. R. Newton, Nucl. Instrum. Methods A **566**, 452 (2006).

[16] T. M. Semkow, G. Mehmood, P. P. Parekh, and M. Virgil, Nucl. Instrum. Methods A **290**, 437 (1990).

[17] S. Carson *et al.*, Nucl. Instrum. Methods A (2010) doi:10.1016/j.nima.2010.02.128.

[18] C. Iliadis *et al.*, Nucl. Phys. A (2010) doi:10.1016/j.nuclphysa.2010.04.010.

[19] C. Iliadis *et al.*, Nucl. Phys. A **512**, 509 (1990).

[20] C. Chronidou, K. Spyrou, S. Harissopulos, S. Kossionides, and T. Paradellis, Eur. Phys. J. A **6**, 303 (1999).

[21] S. Harissopulos, C. Chronidou, K. Spyrou, T. Paradellis, C. Rolfs, W. H. Schulte, and H. W. Becker, Eur. Phys. J. A **9**, 479 (2000).

[22] M. A. Meyer and J. J. A. Smit, Nucl. Phys. A **205**, 177 (1973).

[23] M. Piiparinen, A. Anttila, and M. Viitasalo, Z. Phys. **247**, 400 (1971).

[24] R. Juvet Jr., G. Allmaier, and E. Schmid, Anal. Chem. **63**, 2352 (1991).

[25] V. A. McGlone and P. B. Johnson, Nucl. Instrum. Methods B **61**, 201 (1991).

[26] J. Nash, *Compact Numerical Methods for Computers: Linear Algebra and Function Minimisation* (CRC Press, Boca Raton, FL, 1990).

[27] J. Nelder and R. Mead, Comput. J. **7**, 308 (1965).

[28] J. Ziegler, Nucl. Instrum. Methods B **219**, 1027 (2004).

[29] Z. B. Du Toit, P. R. de Kock, and W. L. Mouton, Z. Phys. **246**, 170 (1971).